Journal of Engineering Mathematics 20 (1986) 271–292

Concerning inviscid solutions for large-scale separated flows

F.T. SMITH

Department of Mathematics, University College London, Gower Street, London WC1E 6BT, England

(Received April 23, 1986)

Summary.

The large-scale separated eddies set up behind a bluff body at high Reynolds number are considered, for steady laminar planar flow. The main eddies are massive and are controlled predominantly by inviscid mechanics, with uniform vorticity inside. Analytical and computational solutions of the massive-eddy (vortex-sheet) problem are then described. A further possibility studied is that, even with lateral symmetry assumed, there may still be an extra degree of nonsymmetry or skewing with respect to the streamwise direction. Small-scale separations, where a Benjamin-Ono equation also possibly yielding nonsymmetric solutions can come into play, are discussed briefly.

1. Introduction

The main concern of this work is the theoretical structure of the large-scale eddies set up in high-Reynolds-number flow, past a bluff body or thick airfoil in a uniform freestream. In particular, a predominantly inviscid massive-eddy account is discussed. There is possible application also to flow past a small step, ramp, thin trailing edge or other obstacle producing smaller-scale eddies.

Depending on the Reynolds number, and with many notable exceptions, such flows in practice often go through transition to turbulence, but that poses difficulties that are, quite simply, beyond current understanding in any firm theoretical sense. Therefore, we turn to an alternative strategy, namely, to try to understand the laminar steady-flow version first. This is itself a fundamental problem, for flow past a circular cylinder for example (Fornberg [1], Smith [11]), and if it cannot be clarified the hope of understanding more complex flows is correspondingly diminished. Once it is clarified, we may then consider the nonlinear stability of the laminar separated version, or rather extend the theory to an unsteady version, subsequently, and examine the unsteady breakdown of the flow. This aspect is pursued by Smith [10], among others. In addition, however, the limiting description for steady flow, when the Reynolds number is large, is a very important one to have available because of its many applications. These are for example, to separated thin-airfoil motions, including hysteresis and stall, which are often observed experimentally; to pointing to appropriate computational methods at finite Reynolds numbers; to providing comparisons or checks on numerical work; to showing the main physical mechanisms which occur, hence yielding deeper understanding; and to providing a basis for studies of unsteady flow properties. Moreover, the predictions from the limiting theory sometimes hold good in a numerical sense at surprisingly low Reynolds numbers.

The Reynolds number Re is assumed to be large, below, and non-dimensional velocities (u, v), Cartesian coordinates (x, y), and pressure p are used such that the freestream velocity is (1, 0), the freestream pressure is zero, and the airfoil chord is 1. The fluid is taken to be incompressible in most of what follows. Section 1 describes previous and recent numerical and analytical studies of the large-scale separated flow past a bluff body, e.g. a circular cylinder. Then in Sections 3 and 4, which are the main body of the work, a proposal concerning a massive eddy-scale flow behind the body, for $\mathrm{Re} \gg 1$, is examined analytically and numerically. The proposal appears to be self-consistent as far as it has been taken to date. In addition, the present computations address the side issue of the existence of an extra degree, or degrees, of freedom in the main, inviscid, massive-eddy/vortex-sheet problem posed. For, even with lateral symmetry in y assumed for the main eddy, nonsymmetry may be possible still (if unlikely) with respect to the streamwise direction x, i.e. the eddy can be "skewed" in the $\pm x$-direction. Further discussion is presented in Section 5, including an alternative approach from the viewpoint of triple-deck theory, for smaller disturbances; there a Benjamin-Ono or similar equation applies and, like its more massive counterparts above, it too may yield nonsymmetric as well as symmetric solutions.

2. Background

On an inviscid basis alone, there are many possibilities that can be considered, and indeed allowed, for the flow past a thick airfoil or bluff body. The following are some of the principal ones (see Figure 1). The first is classical attached motion governed mainly by the potential-flow or Euler equations. A thin viscous boundary layer and subsequent wake are assumed, and if the boundary layer can remain attached, because of smoothed leading-edge and trailing-edge conditions for example, or due to properties of a turbulent boundary-layer model, then the large-Reynolds-number structure of the flow fits together readily and is of a fairly simple hierarchical form, including classical Prandtl boundary-layer theory. Second, if only small separations are present, for instance at a symmetric or nonsymmetric trailing edge, then again the majority of the flow takes the classical hierarchical form, while the small-scale separated motion is described by viscous-inviscid interactive theory of the triple-deck kind or similar. This type of flow is discussed more later on. Third, suppose the separation is instead of large scale, producing eddies whose sizes are comparable with the body size at least. Then one possibility is the Prandtl-Batchelor structure with the typical eddy size being taken to be comparable with the body dimensions and the vorticity in the main part of the eddy being uniform, this analytically from an appeal to viscous forces inside the eddy. A fourth candidate, and likewise a major one in the context of large-scale separated motion, is the extended Kirchhoff structure, where the flow splits into body-scale and (larger) eddy-scale parts with relatively slow flow at constant pressure inside the main eddy. A mixture of essentially the third and fourth candidates above turns out to be of most interest subsequently, in Sections 3 and 4, but at the moment the central point is that according to inviscid theory all the above forms are acceptable and, once discontinuities across vortex sheets are allowed, as seems sensible physically, there are infinitely many inviscid "solutions" for large-scale separating flows.

With all this arbitrariness in purely inviscid theory, it is essential to take account of the effects of viscosity to decide matters more specifically, certainly when solid surfaces are

present. Therefore, we turn first here to the Navier-Stokes equations, taking two dimensional laminar steady motion as a starting point, and examine what happens as the Reynolds number Re increases. Accurate computations, experiments and an asymptotic theory of the extended Kirchhoff kind (Fig. 1, and Smith [9], Fornberg [1]) mentioned previously appear at first sight to fall encouragingly into line for medium values of Re, in the case of symmetric flow past a circular cylinder. The drag coefficient c_D for the cylinder is quite well predicted by that theory, in comparison with reliable Navier-Stokes calculations and with experimental measurements available, for Reynolds numbers as low as about 10 and up to about 300: Smith [9]. The theory here (reviewed by Messiter [5] and Smith [9]) has the Kirchhoff free-streamline form within the body scale, giving rise to an O(1) drag coefficient and a parabolically widening eddy downstream at the onset of the larger eddy scale flow. The latter scale has streamwise extent O(Re), to conserve momentum in the ultimate wake far beyond, the transverse extent is $O(Re^{1/2})$, and the

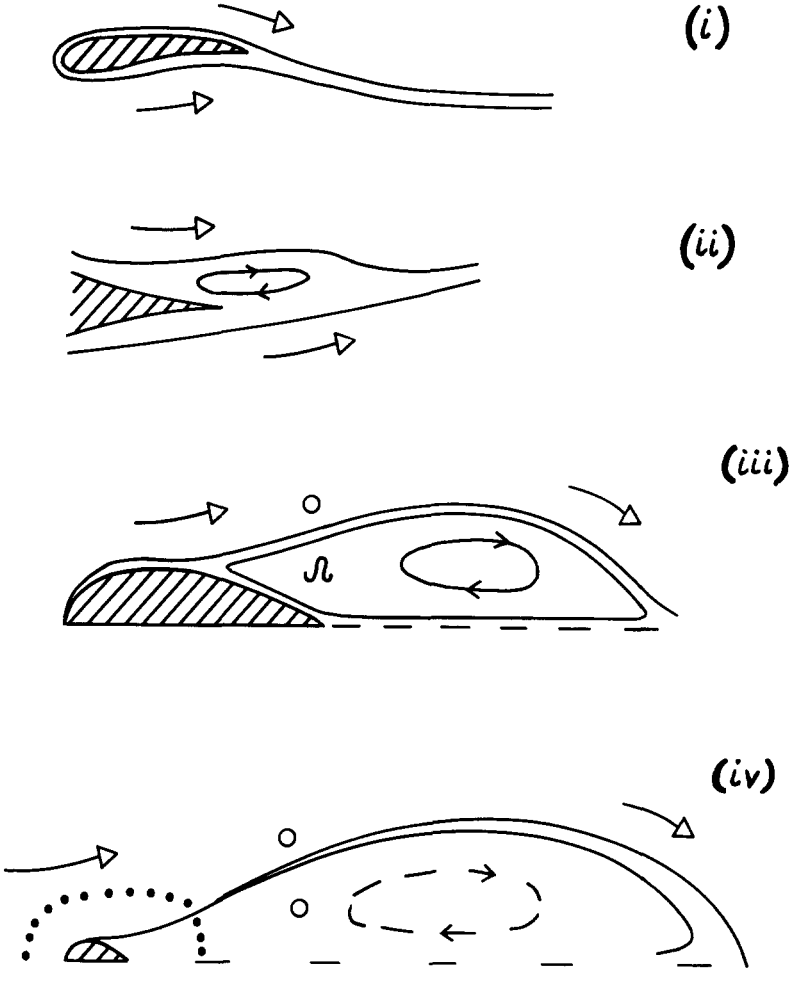

Figure 1(a). Various types of inviscid solutions with small- or large-scale separation present. (i) Attached flow. (ii) Small-scale separation present near a trailing edge. (iii) Prandtl-Batchelor model. (iv) Extended Kirchhoff method.

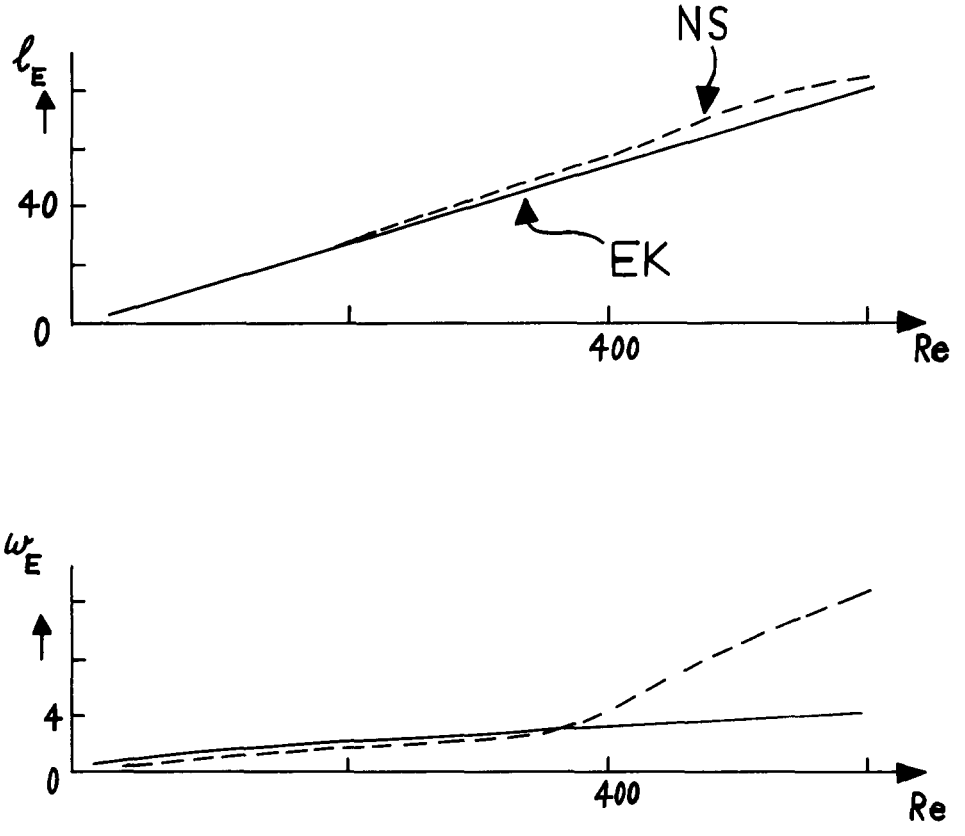

Figure 1(b). Numerical Navier-Stokes results (— — —, Fornberg [1]) for the eddy length l_E and eddy width w_E behind the circular cylinder, including results at higher Re. Extended Kirchhoff theory predicts the solid curves, for comparison.

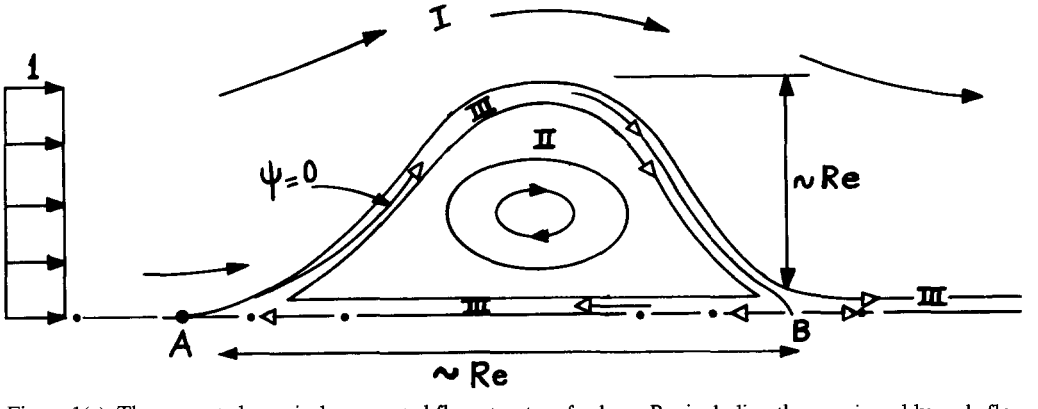

Figure 1(c). The suggested massively-separated flow structure for large Re, including the massive eddy-scale flow I, II addressed in Sections 3 and 4.

eddy shape is an ellipse to preserve uniform pressure at leading order. As noted before, the theory's predictions agree quite well with computations and experiments, and similarly in other flow configurations such as internal motions. But there is a drawback in the

present context of external flow. The drawback (see Smith [9], [11]) arises from the theoretical closure of the eddy, where the free shear layer bounding the eddy is split into two parts by inviscid means, one part going forward into the ultimate wake and the other returning upstream. To conserve vorticity [$\nabla^2\psi$ = function (ψ)] the returning part must have O(1) reversed velocities and O(1) thickness, with a jet-like profile, and so the assumption of relatively slow flow in the eddy, upstream of this, is opened to question, the more so as both the jet and the viscous free shear layer have to draw fluid from the eddy without there being any corresponding source of fluid available. No satisfactory mechanism for completing the account of the entire eddy motion has been found yet and indeed at present this extended Kirchhoff theory appears to be incomplete, for external flows.

That brings us to the more recent computations of the Navier-Stokes equations at higher Reynolds numbers by Fornberg [1] and, at not quite so high Re values, by Ingham [4]. The computations, summarized in Figure 1, show eventually an approximately linear increase of both the eddy length *and* the width, with increasing Re. It should be mentioned that of course there are no laminar-flow experiments, as yet anyway, to compare with at these larger Reynolds numbers because in practice the flow past the cylinder is very unstable then. Nevertheless, the concept of a limiting description for $\mathrm{Re} \gg 1$ is still a most important one to clarify, not least because of its applications to separated airfoil motions, including, e.g., hysteresis and stall, to suggesting appropriate numerical methods, its highlighting of the physical mechanisms involved, and as a basis for unsteady-flow studies: see Section 5. The asymptotic theory (Smith [8], [11]) to which the above calculations point, and which replaces the extended Kirchhoff description, is based on a *massive* eddy size of dimensions O(Re) by O(Re): Figure 1. With such dimensions, the induced pressure and velocities inside the eddy are O(1) and so, in contrast with the earlier account, the eddy motion now affects the viscous shear layer and the viscous return wake substantially, and the earlier-noted contradiction at eddy closure and the difficulties concerning entrainment are thereby avoided.

The properties of the large-scale separated flow structure are described in the following two sections.

3. Large-scale structure and inviscid solutions

The limiting structure as far as the main eddy is concerned is based on Sadovskii's [7] model but supplemented by viscous effects. The major difference from the earlier theory is that now the recirculating eddy motion in zone II is supposed to be as strong as the external motion in zone I and so it affects the viscous-layer flows III substantially (Smith [8], [11]). In the inviscid regions I, II of Figure 1 we have

$$\nabla^2\bar{\psi} = 0 \quad (\text{in I}), \quad \nabla^2\bar{\psi} = -\bar{\Omega} \quad (\text{in II}) \tag{3.1}$$

for the stream function $\bar{\psi} \sim \mathrm{Re}^{-1}\psi$ in scaled terms, with $\mathrm{Re}^{-1}\bar{\Omega}$ being the small negative uniform vorticity. At the vortex sheet $Y = S(X)$, which is the unknown boundary between I, II,

$$\bar{\psi},\ p \quad \text{are continuous } (Y = S(X)\pm); \tag{3.2}$$

and the end conditions, which play a significant role, require

$$\text{tangential departures at } X = 0,\ L, \tag{3.3}$$

where X, Y are O(Re)-scaled coordinates and Re L is the eddy length. The other boundary conditions relevant impose a streamline along the X-axis and the uniform stream in the farfield.

Generally the flow speeds q_{I}, q_{II} on either side of the vortex sheet are unequal. The whole inviscid solution then depends on the parameter C_{II}, that is, the pressure at the ends $X = 0$, L of the eddy where $q_{\mathrm{II}} \to 0$; here $C_{\mathrm{II}} = (q_{\mathrm{II}}^2 - q_{\mathrm{I}}^2 + 1)/2$ from Bernoulli's theorem, and the constant C_{II} can take values between zero and $1/2$. The inviscid problem, which is our main concern here, determines the product $\bar{\Omega}L$ for a prescribed value of C_{II}, but subject to a symmetry assumption as discussed later in this section and in Section 4. Let us confine attention for the moment to those solutions of the inviscid problem, in (3.1)–(3.3), which are symmetric in X about the eddy-center station $X = L/2$.

As expected in view of earlier comments, there is still a wide range of solutions available, on inviscid grounds. Next, however, the properties of the three viscous layers III_1, III_2, III_3 in Figure 1 narrow the choice. These layers are all governed by the boundary-layer equations. The requirement of periodicity (Smith [8]), i.e. continuity around the viscous layers III_1 (the free shear layer or vortex sheet) and III_2 (the return wake), which border the eddy, is expected to fix the functional dependence of L and C_{II} on $\bar{\Omega}$, leaving only $\bar{\Omega}$ unknown. Also, a left-over jet with O(1) velocities and thickness is sent back from layer III_2 into the body-scale flow (see below), whereas the ultimate wake, which is the third viscous layer III_3 downstream, determines the drag coefficient c_D as a function of $\bar{\Omega}$ by means of the overall momentum balance. At this stage therefore we are left with, in effect, one relation short to completely determine the motion.

The extra relation required comes from consideration of the body-scale motion, sketched in Smith [8], [11]. Its main feature is that the eddy motion, turning there, again has significant vorticity (now O(1)) but the vorticity is nonuniform, being caused by the left-over jet from the larger-scale motion. Apart from that, the body-scale structure is very like the Kirchhoff free-streamline form and produces an O(1) drag coefficient c_D, as well as a parabolic growth of the eddy width downstream. The whole flow structure in fact is something of a mixture of the extended Kirchhoff and the Prandtl-Batchelor forms.

Some more details of the body-scale flow are the following (see also Smith [8], [11])). (a) The flow is subjected to a reduced freestream in effect, in that

$$u \to (1 - 2C_{\mathrm{II}})^{1/2},\ p \to C_{\mathrm{II}}$$

in the farfield, to match with the eddy-scale flow. (b) The main inviscid regions IV, V in the last-named reference are governed by conservation of vorticity. Here the vorticity in the reversing-flow region V stems from the viscous return-jet profile $u(0+, y)$ of the eddy-scale motion in layer III_2 and it sets up a significant eddy flow to be turned forward in region V. (c) The separation (near the point C of Figure 3 of Smith [11]) is "smooth" and described by triple-deck theory; see also Section 5, and the comparison with experiments in Smith [8]. The smoothness requirement plays a part in fixing the body-scale solution. (d) Secondary separation is likely in the backward boundary layer approaching separation but there is some question as to whether this separation is relatively small or not. (e) Because the eddy width grows like $x^{1/2}$ downstream, buffer

zones are necessary to join certain aspects of the body- and eddy-scale flows. (f) The body-scale problem determines c_D as a function of $\bar{\Omega}$, since the vorticity in region V depends on $\bar{\Omega}$. This provides the final relation necessary to fix c_D, $\bar{\Omega}$, L and C_{II}. Also no difficulty occurs now during the eddy closure process, since a backward jet is an admissible feature of the present flow structure: see Figure 4 of Smith [11].

The first task, then, is to solve the inviscid problem of the massive-eddy motion, the second task is to calculate the viscous-layer problems (layers III), and the third task is to solve for the body-scale flow.

Concerning the first task, for which numerical results are described subsequently, and which forms the basis of the present study, we note that Sadovskii [7] obtained a few solutions near one end of the range (C_{II} near $1/2$), while at the other end, for C_{II} small, there is a thin-eddy limit (Smith [11]) which is helpful analytically, as well as having application in Section 5 below. For small values of C_{II}, or relatively large vorticity, the equation of constant vorticity inside the eddy reduces to $\partial^2\bar{\psi}/\partial Y^2 = -\bar{\Omega}$ since the eddy is relatively thin, and so, from integration, the eddy pressure $p_{II}(X)$ and the eddy shape $S(X)$ are related by

$$p_{II}(X) = C_{II} - \tfrac{1}{8}\bar{\Omega}^2 S^2(X). \tag{3.4}$$

But the external motion past the thin eddy yields the surface pressure, in terms of a Cauchy-Hilbert principal value,

$$p_I(X) = -\frac{1}{\pi}\int_0^L \frac{S'(\xi)\,d\xi}{(X-\xi)}. \tag{3.5}$$

Hence continuity of pressure leads to the nonlinear integro-differential equation

$$\tfrac{1}{8}\bar{\Omega}^2 S^2(X) - C_{II} = \frac{1}{\pi}\int_0^L \frac{S'(\xi)\,d\xi}{(X-\xi)} \tag{3.6a}$$

for the unknown eddy shape $S(X)$ between $X = 0$, L subject to the constraints

$$S = S' = 0 \quad \text{at } X = 0,\ L. \tag{3.6b}$$

The above is an integrated steady form of the Benjamin-Ono equation. Further analysis e.g. using Fourier series may be possible, but computation seems most desirable for later purposes. The computations were performed initially by means of a Carter-like approach as follows (also see Section 4). A guess is made for $S(X)$, then $p_{II}(X)$, $p_I(X)$ are calculated from (3.4), (3.5) respectively, and the pressure difference $(p_I - p_{II})$ is used as the basis for updating $S(X)$, and so on. The updating takes the new S as a linear combination of the old S and $(p_I - p_{II})$, at each X, in such a way that short-scale wave growth is avoided. Also, a normalization including setting $L = 2$ is applied to avoid the trivial solution $C_{II} = S(X) = 0$. It is noted here that Sadovskii [7] uses a parameter for these flows which is inappropriate as in effect it produces dual solutions, unlike with the parameter C_{II}. Solutions of the thin-eddy case (3.6a, b) are shown in Figure 5 of Smith [11] with $\hat{S}$, $\hat{p}$ denoting normalized variables and with symmetry about the eddy centre.

When two characteristic properties of the full problem are plotted (last reference, and Fig. 2 below), namely the maximum eddy width and a measure of the vorticity, the

comparison between the thin-eddy predictions for small C_{II} and Sadovskii's results near $C_{II} = 1/2$ is found to be fairly close. So the thin-eddy theory seems useful in numerical terms (see next–but–one paragraph), in addition to giving more analytical backing to the whole model and having relevance to the smaller-scale separations discussed in Section 5.

A possibility noted here is that the thin-eddy or other solutions of the massive-eddy problem may open the door to Prandtl-Batchelor solutions. No solutions of the Prandtl-Batchelor type for flow past a smooth body have been found yet, as far as we know, even on an inviscid basis, let alone allowing for viscous effects. Yet it is possible that a smooth thin body can be inserted near the start of the massive eddy without drastically disrupting the flow structure. The same conclusion holds if a thin body is placed along the x-axis even in the middle of the eddy, certainly in the thin-eddy case. Again, a small Prandtl-Batchelor eddy adjoining a smooth airfoil surface is governed by the thin-eddy analysis. So continuation would tend to suggest the existence of Prandtl-Batchelor flows having eddy sizes comparable with the airfoil dimensions, at least on inviscid grounds.

Returning to the massive-eddy problem (3.1)–(3.3) for general values of C_{II}, we have obtained solutions by a numerical procedure outlined in (A)–(F) below. This is built on the thin-eddy method since as noted above that gives a good first estimate numerically for the entire range of values of C_{II}. More details of the method are given in Section 4.

(A) Specify C_{II} and guess $S(X)$, $\bar{\Omega}L$.

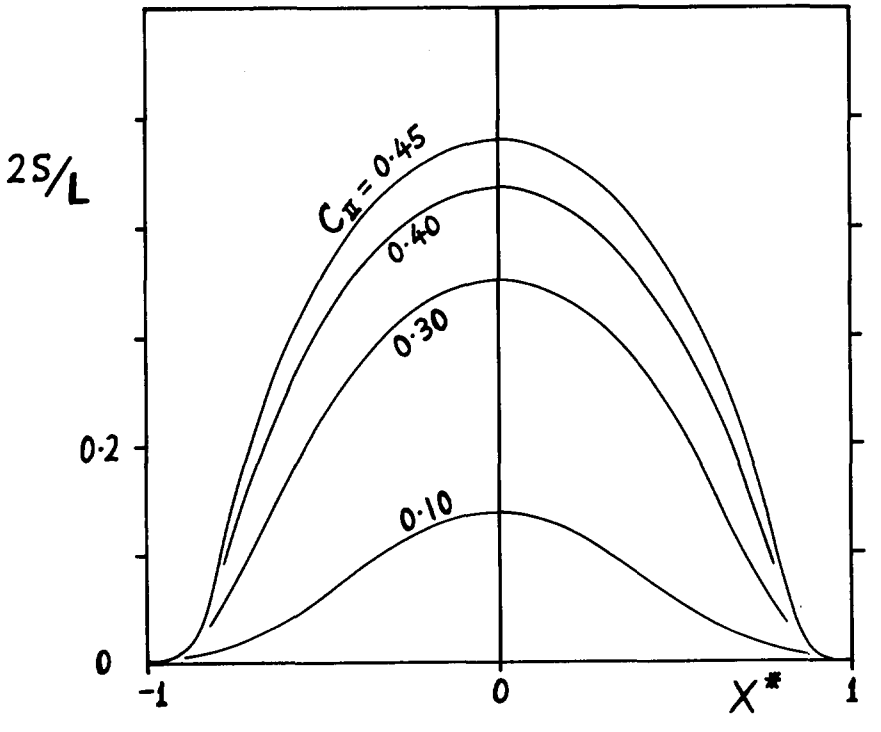

Figure 2. Present solutions of (3.1)–(3.3) for (a) the eddy shape and (b) the boundary pressure, versus $X^* = 2X/L - 1$, for various values of the end-pressure parameter C_{II}; and (c) the maximum eddy width $L^{-1}S(X^* = 0)$ and vorticity $\bar{\Omega}L/2$ as C_{II} varies [●, ○ present work; ×, ⊙, from Sadovskii [7]; — — —, from thin-eddy limit]. These are symmetric solutions.

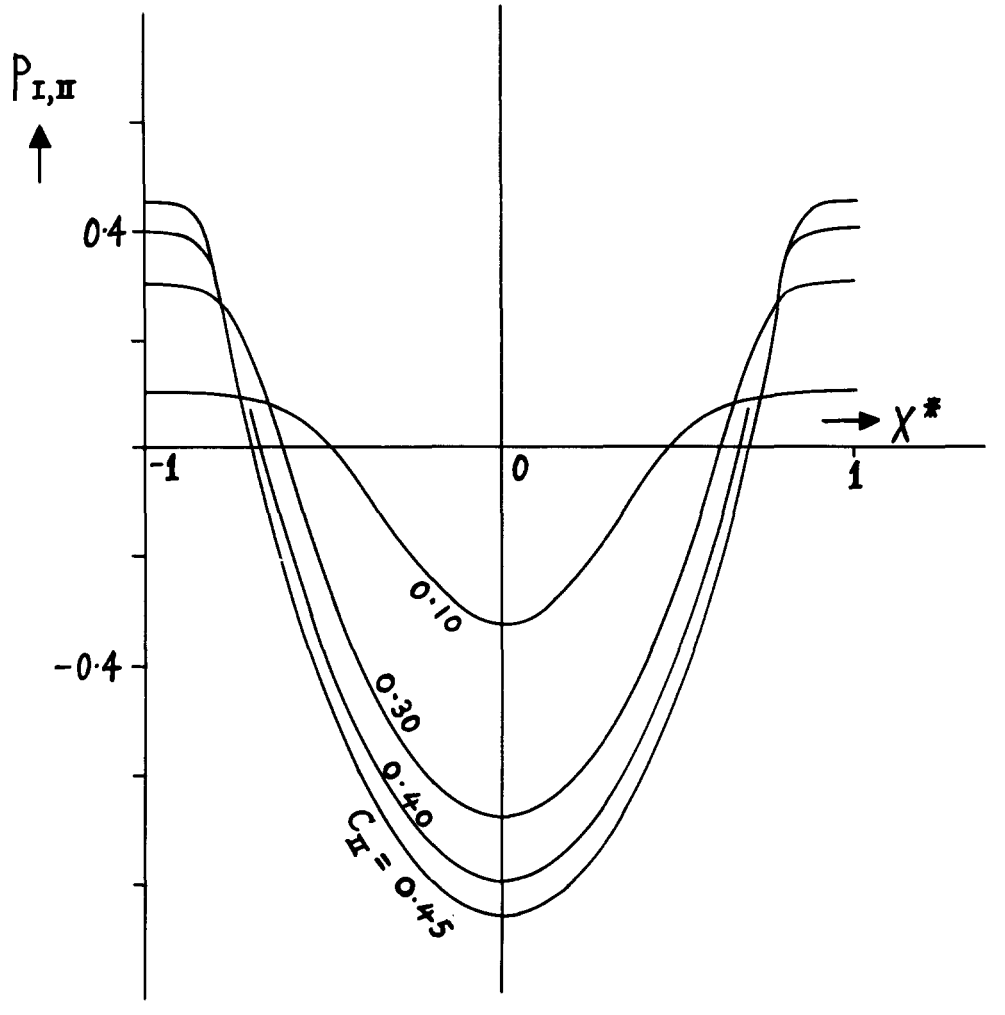

Fig. 2b.

(B) Take the thin-eddy formula (3.5) for p_I first and iterate to include full nonlinearity, using Cauchy-Hilbert type of integrals throughout.

(C) Next, take the thin-eddy formula (3.4) for p_{II} and iterate to include full nonlinearity, using an S.O.R. scheme with the coordinate $Y/S(X)$.

(D) Update $S(X)$ by a Carter technique, in the form $S^{(n)} = S^{(n-1)} + r(p_I - p_{II})$ at each X, where r is a relaxation factor and (n) denotes the level of the sweep.

(E) Renormalize to update $\bar{\Omega}L$ by imposing the conditions (3.3).

(F) Return to (B), until convergence is achieved.

The scheme works reasonably well, certainly at lower values of the parameter C_{II}, although the convergence at higher values of C_{II} has proved slow so far. Improvements of the method and alternatives, e.g., a Veldman-Davis scheme, are considered in Section 4.

The results obtained are summarized in Figures 2, 3. It should be stressed here that generally these are solutions extrapolated from converged results on a number of grids: see also above and Figure 4 below. The results in Figure 2, for values of C_{II} up to 0.45,

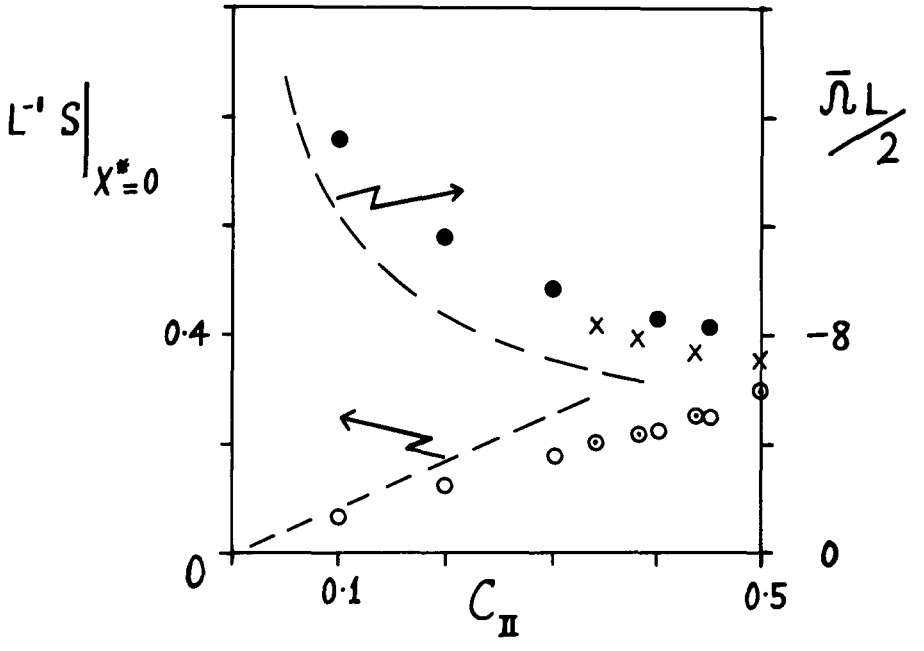

Fig. 2c.

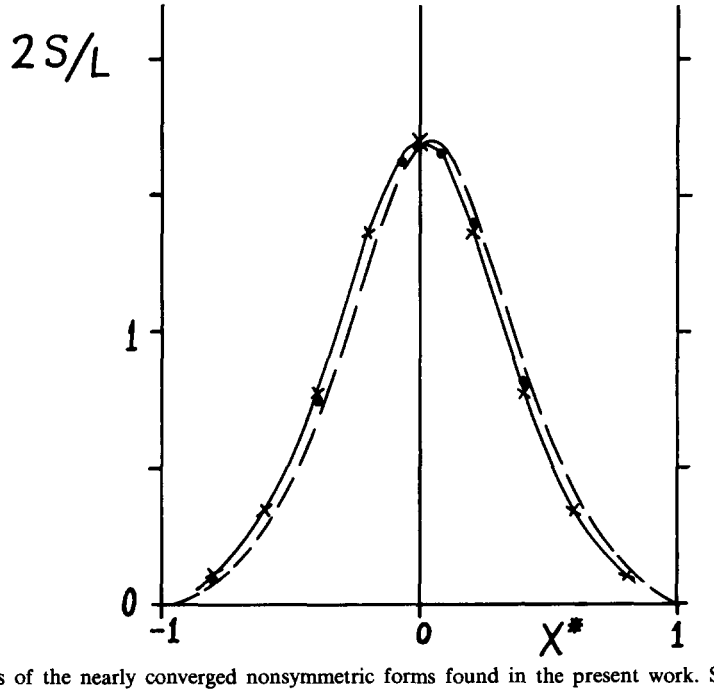

Figure 3. Samples of the nearly converged nonsymmetric forms found in the present work. See also a later footnote. For the *thin*-eddy case (3.6), (a) and (b) show the eddy shape and boundary pressure, versus X^*, when the nonsymmetry parameter $\lambda_1 = 0$, 0.1, 0.2 [—×—, ●, — — — respectively]. For the *massive*-eddy problem (3.1)–(3.3), with $C_{II} = 0.4$, (c) and (d) give the eddy shape and boundary pressure when $\lambda_1 = 0$[—×—], 0.1 [●], 0.2 [— — —]. Note that these inviscid forms are reversible about $X^* = 0$: see also the text.

approach the earlier ones for the thin-eddy case, as C_{II} is decreased, and they are also near Sadovskii's [7] results at higher values of C_{II}. The limiting case of $C_{II} = 1/2$ (Pierrehumbert [6]) is an interesting one, by the way, partly because it has no discontinuity in velocity across the bounding vortex sheet, so that the speed driving the body-scale flow is reduced by an order of magnitude, probably (but not necessarily) producing an asymptotically small drag c_D. Further, Fornberg's [1] Navier-Stokes calculations may be tending to point towards that limiting case, or near it, as regards the eddy width/length ratio: we would refer here also to the comments at the end of the next paragraph.

The results in Figure 3, however, concern a new feature that was studied in the calculations. This is that there might be a host of *nonsymmetric* solutions of the inviscid massive-eddy problem (3.1)–(3.3), in addition to the symmetric ones of Figure 2. Here the nonsymmetry refers to "skewing" in the X-direction, i.e. nonsymmetry about $X = L/2$; symmetry about the wake center-line $Y = 0$ is preserved throughout. These possibly extra, nonsymmetric, solutions in Figure 3 were obtained in exactly the same way numerically as the symmetric ones in Figure 2 except that the starting guess for $S(X)$ was taken to be nonsymmetric and the convergence criterion used previously was relaxed (see also a later footnote). A symmetry condition imposed implicitly in the calculations reported in Smith [11] was also removed here: see also Section 4. As figure 3 shows, the nearly converged nonsymmetric solutions are present both for the thin-eddy problem (3.6a, b) and for the

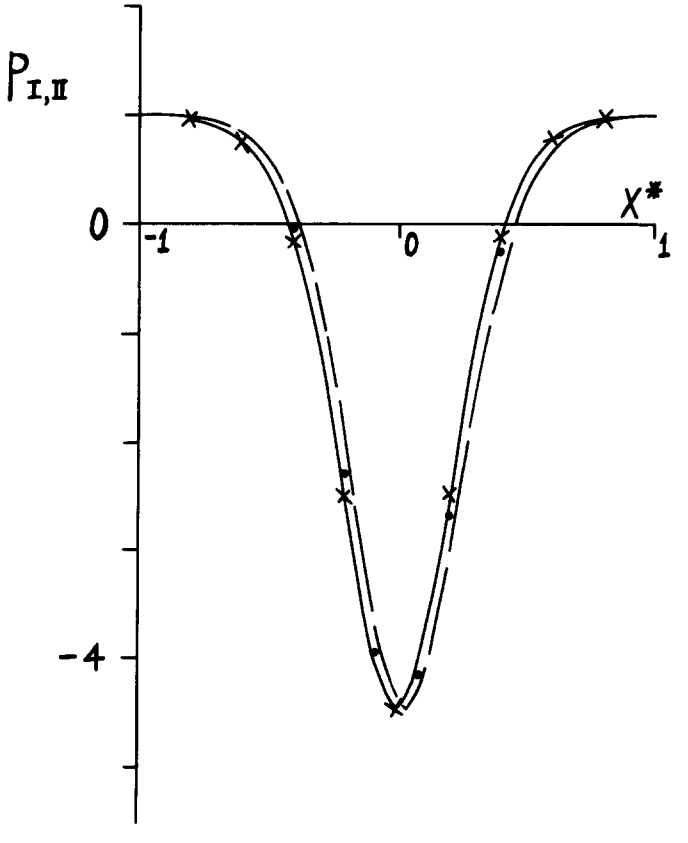

Fig. 3b.

full massive-eddy problem (3.1)–(3.3). Moreover, the above skewed forms alter the maximum eddy width and the vorticity a little relative to the symmetric ones and this leads to the possibility that the Navier-Stokes calculations of Fornberg [1] are not necessarily pointing strongly to the symmetric-eddy limit solution of Pierrehumbert [6] but rather perhaps to a nearby nonsymmetric-eddy solution.

The task of using these inviscid solutions as input for the viscous-layer problems, to determine $c_D(\bar{\Omega})$ and $L(\bar{\Omega})$, has still to be addressed seriously. So has the body-scale problem fixing c_D, L, $\bar{\Omega}$. The overall picture so far, however, looks reasonably promising, we feel, despite the possibility of an extra degree or degrees of freedom introduced by the nonsymmetry found above (see footnote later).

4. Numerical method

The numerical method used for solving the *massive-eddy problem* (3.1)–(3.3) follows the plan (A)–(F) outlined near the end of Section 3. Alternative methods for this type of vortex-sheet calculation are given in Sadovskii [7] and Pierrehumbert [6], for example. Our approach, however, is built on the thin-eddy method in Smith [11] in view of the latter's

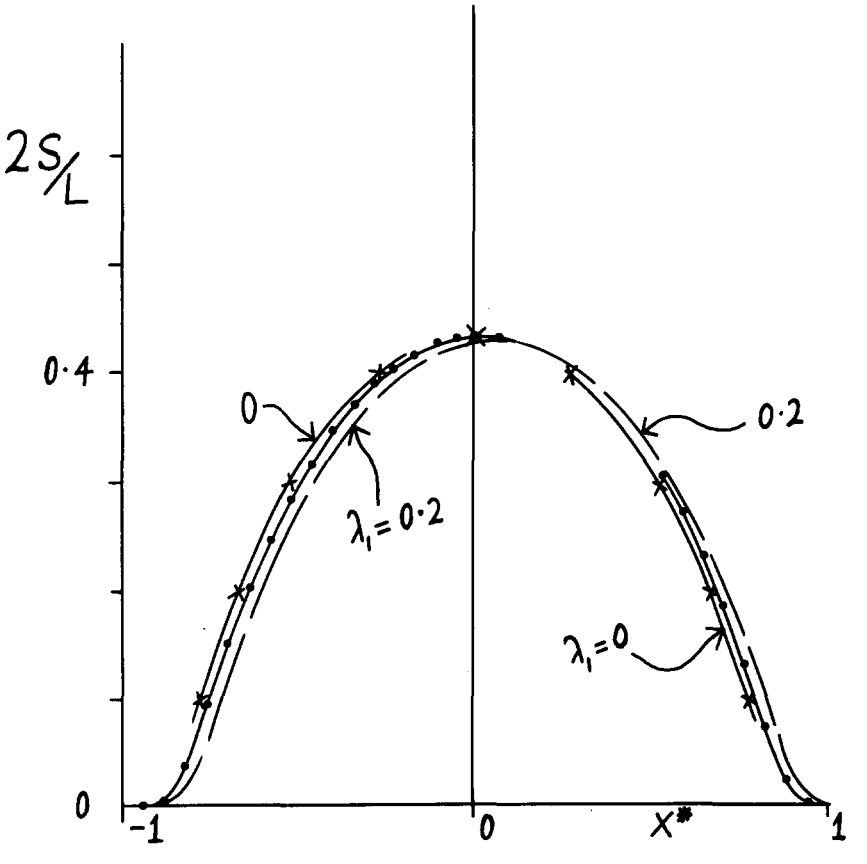

Fig. 3c.

already-good predictions referred to in the previous section. In the present section fuller details of each of the steps (A)–(F) are presented.

Step (A)

The values specified for the parameter C_{II} were in the range 0.1–0.45. The starting guesses for $S(X)$ were of the form

$$\frac{2S(X)}{L} = C_{II}(1 - X^{*2})^{3/2}(1 - \lambda_1 X^*)\{\,|\,X^*\,| \leqslant 1\} \tag{4.1}$$

with $\lambda_1 = 0$ for the symmetric solutions but with λ_1 taking positive values between 0 and 0.2 for nonsymmetric cases, while $-\bar{\Omega}L/2$ was given a typical guessed value of 1. Here we normalize L to be equal to 2, or, equivalently, set $(X, Y, S) = L(X^* + 1, Y^*, S^*)/2$, $\bar{\Omega} = 2\bar{\Omega}^*/L$, $\bar{\psi} = L\bar{\psi}^*/2$ and solve for the asterisked variables. The asterisk is omitted henceforth, for convenience; the *shift of the X-origin to the mid-section of the eddy* is kept.

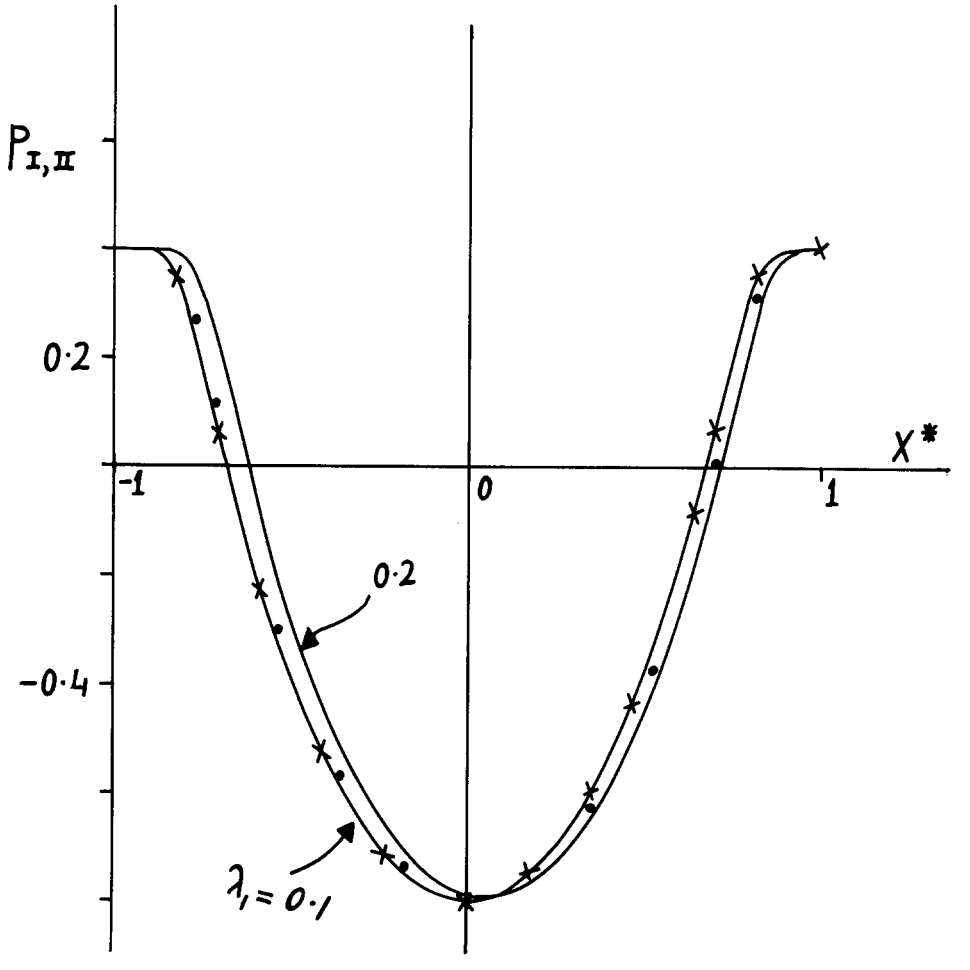

Fig. 3d.

Step (B)

Given the latest $S(X)$ distribution, the aim in this step is to work out first the unknown values of the effective slip $\bar{u}(X, 0)[\equiv 1 + g(X)$, say] and upwash $\bar{v}(X, 0)[\equiv h(X)$, say] along the axis $Y = 0$, using complex-variable properties in the outer flow I. Here $(\bar{u}, \bar{v})$ is the velocity $(\partial\bar{\psi}/\partial Y, -\partial\bar{\psi}/\partial X)$. Since $h(X)$ is zero for $|X| > 1$, and the complex function $(\bar{u} - 1 - \mathrm{i}\bar{v})$ is analytic in $z \equiv x + \mathrm{i}Y$ and vanishes at infinity, Cauchy's integral formulae give

$$g(X) = \frac{1}{\pi} \int_{-1}^{1} \frac{h(\xi)\, \mathrm{d}\xi}{(X - \xi)}, \tag{4.2}$$

$$\bar{u}(X, S(X)) - 1 = \frac{1}{\pi} \int_{-1}^{1} \frac{h(\xi)(X - \xi)\, \mathrm{d}\xi}{(X - \xi)^2 + S^2(X)} \{\equiv g(X) + R_2(X) \text{ say}\}, \tag{4.3a}$$

$$\bar{v}(X, S(X)) = \frac{S(X)}{\pi} \int_{-1}^{1} \frac{h(\xi)\, \mathrm{d}\xi}{(X - \xi)^2 + S^2(X)} \{\equiv h(X) + R_3(X) \text{ say}\}. \tag{4.3b}$$

The equalities in curly brackets in (4.3) give the definitions of the functions $R_{2,3}$. From (4.3), the streamline condition in (3.2), i.e. $\bar{v}/\bar{u} = S'(X)$ at $Y = S(X)$, requires

$$R_1 = -R_3 + S'(g + R_2) \quad \text{for } |X| < 1 \tag{4.4}$$

where R_1 is defined by

$$h = S' + R_1 \quad \text{for } |X| < 1. \tag{4.5}$$

So, with an initial guess [e.g. zero as in the thin-eddy problem] or latest iterate for the $R_1(X)$ distribution, (4.5) allows $h(X)$ to be evaluated; then $g(X)$ follows from (4.2); then (4.3a, b) yield updated $R_{2,3}(X)$ distributions; and new $R_1(X)$ values are then implied by (4.4). This iteration of (4.2)–(4.5) is repeated a number of times until a convergence criterion on the successive iterates is satisfied.

Once convergence is achieved, the boundary pressure $p = p_1$ at $Y = S(X) +$ is obtained as

$$p_1(X) = \tfrac{1}{2}\left\{1 - (1 + S'^2)(1 + R_2 + g)^2\right\}, \tag{4.6}$$

from use of Bernoulli's law.

The discretizations adopted for the integral formulae (4.2), (4.3a, b) respectively are, with suitable centering aimed at diagonal dominance,

$$g_i = \frac{1}{\pi} \sum_{j=2}^{K-1} \frac{(i - j)h_j}{\left[(i - j)^2 - \frac{1}{4}\right]}, \tag{4.7}$$

$$R_{2i} = -g_i + \frac{\Delta X}{2\pi} \sum_{j=2}^{K} \frac{(h_j + h_{j-1})(X_i - X_{j-\frac{1}{2}})}{\left[(X_i - X_{j-\frac{1}{2}})^2 + S_i^2\right]}, \tag{4.8a}$$

$$R_{3i} = -h_i + \frac{h_i}{\pi}\left\{\tan^{-1}\left(\frac{1 - X_i}{S_i}\right) + \tan^{-1}\left(\frac{1 + X_i}{S_i}\right)\right\}$$

$$+ \frac{S_i\,\Delta X}{\pi}\left\{\sum_{j=2}^{K-1} \frac{(h_j - h_i)}{\left[(X_i - X_j)^2 + S_i^2\right]} - \tfrac{1}{2}h_i/\left[(X_i - 1)^2 + S_i^2\right]\right.$$

$$\left. - \tfrac{1}{2}h_i/\left[(X_i + 1)^2 + S_i^2\right]\right\}, \tag{4.8b}$$

while standard second-order-accurate differencing is applied to the equations (4.4)–(4.6). Here a uniform grid-spacing ΔX in X is taken, the subscript i denotes evaluation at the ith station, and i runs from 1 (at $X = -1$) to K (at $X = 1$), so that $(K-1)\,\Delta X = 2$. Also, in (4.8b) an extra $h(X)$ factor is extracted from the integral to increase the accuracy of the numerical integration when $S(X)$ is small.

Step (C)

To solve numerically for the inviscid eddy flow II, again with $S(X)$ prescribed, we write $\eta = Y/S(X)$ and set $\bar{\psi} = S^2(X)\phi$. Then (3.1) yields the equation

$$(1 + \eta^2 S'^2)\frac{\partial^2 \phi}{\partial \eta^2} + S^2 \frac{\partial^2 \phi}{\partial X^2} = -\bar{\Omega} - \left\{4SS'\frac{\partial \phi}{\partial X} + 2(S'^2 + SS'')\phi\right.$$

$$\left. - 2\eta S'S\frac{\partial^2 \phi}{\partial \eta\,\partial X} - \eta(S''S + 2S'^2)\frac{\partial \phi}{\partial \eta}\right\} \tag{4.9}$$

for $\phi(X, \eta)$. This is treated iteratively by use of line-by-line over-relaxation, as opposed to the option of complex-variable theory. A first guess $\bar{\Omega}(\eta^2 - \eta)/2$ [corresponding to the thin-eddy limit] or latest estimate for ϕ is taken. Then (4.9) is replaced by its discrete form

$$\beta\phi_{i,j-1} + \phi_{i,j} + \beta\phi_{i,j+1} = \frac{\left[S_i^2(\phi_{i+1,j} + \phi_{i-1,j})/(\Delta X)^2 + \text{“rest”} + \bar{\Omega}\right]}{2\left[S_i^2/(\Delta X)^2 + \text{“eff”}/(\Delta\eta)^2\right]} \tag{4.10a}$$

where

$$\text{“eff”} = 1 + \eta^2 S'^2, \tag{4.10b}$$

$$\text{“rest”} = 2S_iS'(\phi_{i+1,j} - \phi_{i-1,j})/\Delta X + 2(S'^2 + S_iS'')\phi_{i,j}$$

$$- \eta S_iS'(\phi_{i+1,j+1} - \phi_{i-1,j+1} - \phi_{i+1,j-1} + \phi_{i-1,j-1})/(2\,\Delta X\,\Delta\eta)$$

$$- \eta(S_iS'' + 2S'^2)(\phi_{i,j+1} - \phi_{i,j-1})/(2\,\Delta\eta), \tag{4.10c}$$

$$\beta = \frac{-\text{"eff"}/(\Delta\eta)^2}{2\left[S_i^2/(\Delta X)^2 + \text{"eff"}/(\Delta\eta)^2\right]}, \tag{4.10d}$$

$$S' \to \frac{S_{i+1} - S_{i-1}}{2\,\Delta X}, \quad S'' \to \frac{S_{i-1} - 2S_i + S_{i-1}}{(\Delta X)^2}, \tag{4.10e}$$

$$\eta \to (j-1)\,\Delta\eta, \tag{4.10f}$$

for $2 \leqslant i \leqslant K-1$ and $2 \leqslant j \leqslant J-1$. Here $\Delta\eta = 1/(J-1)$ is the η-step. Equation (4.10a) is solved for the $\phi_{i,j}$'s on the left-hand-side at a particular i value, involving inversion of a tridiagonal matrix, with the right-hand side and the coefficients β assumed known at their latest values. The boundary conditions here are $\phi = 0$ at $\eta = 0$, $1[\phi_{i,1} = \phi_{i,J} = 0]$, and $\phi = \bar{\Omega}(\eta^2 - \eta)/2$ at $X = \pm 1$. Over-relaxation is applied in the updating of all the $\phi_{i,j}$ at the station i. The station is then swept repeatedly through the flow domain until a convergence criterion on the successive iterates is met.

At that stage, the internally produced pressure $p = p_{\text{II}}$ on the eddy boundary at $Y = S(X) -$ follows as

$$P_{\text{II}}(X) = C_{\text{II}} - \tfrac{1}{2}(1 + S'^2)S^2\left[\frac{\partial\phi}{\partial\eta}(X, 1)\right]^2, \tag{4.11}$$

again from Bernouilli's law, at each X station.

Step (D)

The updated $S(X)$ distribution, $S^{(n)}$ say, is obtained in Carter fashion from the old $S^{(n-1)}$ distribution by setting

$$S^{(n)} = S^{(n-1)} + r(p_{\text{I}} - p_{\text{II}}) \tag{4.12}$$

at each X. This of course is equivalent to an explicit time-marching treatment of the artificial-time equation $\partial S/\partial t = (p_{\text{I}} - p_{\text{II}})$, with the pressure-match condition $p_{\text{I}} = p_{\text{II}}$ in (3.2) to be hoped for as the large-time/iterative-convergence limit. The positive sign taken for the time marching here is chosen to avoid any fast-scale instabilities, as dictated by a linear-stability analysis. At the end points $X = \pm 1$ the constraints $S_1 = S_K = 0$ are enforced, in line with (3.3).

Step (E)

This step involving renormalization is an important part of the procedure. The approach is to determine the local behavior of the solution near the end points $X = \pm 1$, in terms of the unknown vorticity $\bar{\Omega}$, and then impose the tangential-departure conditions (3.3) to update $\bar{\Omega}$. In both the symmetric and the possible nonsymmetric solutions these conditions amount to a single equation governing $\bar{\Omega}$.

The function $\mathcal{F}(z) \equiv [(z+1)/(z-1)]^{1/2}(\bar{u} - 1 - \mathrm{i}\bar{v})$ in the outer potential flow is analytic in z and tends to zero at infinity. Moreover, along the axis $Y = 0$,

$$\text{Imag}(\mathcal{F}(z)) = 0 \quad [\text{for } |X| > 1], \quad \left(\frac{1+X}{1-X}\right)^{\frac{1}{2}} g(X) \quad [\text{for } |X| < 1], \tag{4.13a}$$

$$\text{Real}(\mathcal{F}(z)) = \left(\frac{1+X}{1-X}\right)^{\frac{1}{2}} h(X) \quad [\text{for } |X| < 1], \tag{4.13b}$$

because of lateral symmetry in Y for $|X|<1$. Hence Cauchy principal values give the relation

$$h(X)=-\frac{1}{\pi}\left(\frac{1-X}{1+X}\right)^{\frac{1}{2}}\int_{-1}^{1}\frac{g(\xi)}{(X-\xi)}\left(\frac{1+\xi}{1-\xi}\right)^{\frac{1}{2}}\mathrm{d}\xi \tag{4.14}$$

for $|X|<1$. Requiring zero upwash h at $X=-1(+)$, which is equivalent to the tangency condition (3.3), therefore yields

$$\int_{-1}^{1}\frac{g(\xi)\,\mathrm{d}\xi}{(1-\xi^2)^{\frac{1}{2}}}=0. \tag{4.15}$$

The same relation (4.15) results from the tangency condition at $X=1(-)$ when $z\pm1$ are interchanged in the above reasoning. In (4.15) we now set

$$g=-p_{\mathrm{I}}-R_2+R_4 \tag{4.16a}$$

where $R_4(X)$ is defined from (4.6) by

$$R_4\equiv g+R_2+\tfrac{1}{2}-\tfrac{1}{2}(1+S'^2)(1+R_2+g)^2. \tag{4.16b}$$

Then in (4.16a) we may replace p_{I} by p_{II}, in anticipation of the converged solution, and so (4.15) becomes, after manipulation,

$$\tfrac{1}{8}\bar{\Omega}^2\int_{-1}^{1}\frac{S^2(\xi)\,\mathrm{d}\xi}{(1-\xi^2)^{\frac{1}{2}}}=\pi C_{\mathrm{II}}+\int_{-1}^{1}\frac{[R_2(\xi)-R_4(\xi)+R_5(\xi)]\,\mathrm{d}\xi}{(1-\xi^2)^{\frac{1}{2}}} \tag{4.17}$$

where

$$R_5\equiv p_{\mathrm{II}}-C_{\mathrm{II}}+\tfrac{1}{8}\bar{\Omega}^2S^2. \tag{4.18}$$

The requirement (4.17) is imposed to update $\bar{\Omega}(<0)$, with $S(X)$ and all terms on the right-hand side taking their latest known values. This device is designed about the thin-eddy approach noted earlier, like other parts of the entire scheme, and it proved convergent within the overall scheme.

The discretizations representing the integrals in (4.17) were of the trapezoidal kind as in step (B).

Step (F)

This step is just as stated in Section 3. Typically 3000 sweeps of the steps (B)–(F) were required for convergence of symmetric solutions to within a tolerance 10^{-5} in the vorticity $\bar{\Omega}$, with the relaxation factor r in (4.12) typically being 0.001. For the nonsymmetric forms, by contrast, the approach to a converged state was much slower, as it was also for increased C_{II}, and the tolerance had to be raised. For this reason, and because we feel that the nonsymmetric starting solutions could in fact be converging very slowly to a symmetric form instead (see footnote below), we refer to the nonsymmetric forms as

nearly converged and must regard them as conjectures still. A further point is that sometimes during the sweeps we took the modulus of the right-hand side in (4.12), or changed the sign of r, whenever $S^{(n-1)}$ became negative, temporarily, again to prevent short-scale growth locally.

The same scheme (A)–(F) applies also to the *thin-eddy limit problem* (3.6a, b), although that is simpler because the "remainder" terms $R_n (n = 1 \text{ to } 5)$ in (4.3), (4.5), (4.16b), (4.18) are all zero then and so steps (B), (C) above reduce to the explicit formulae (3.5), (3.4) in turn. We also developed, however, an alternative scheme of the Davis [3]-Veldman [12] type for the thin-limit problem. In this alternative scheme (3.6a) is tackled directly, at each $X = X_i$, in the diagonally dominant form

$$\tfrac{1}{8}\bar{\Omega}^2 S_i^2 - C_{\mathrm{II}} = \frac{1}{\pi \Delta X}\left[4S_i - \sum_{\substack{j=2 \\ j \neq i}}^{K-1} \frac{S_j}{(i-j)^2 - \frac{1}{4}}\right] \tag{4.19}$$

where, in effect, $C_{\mathrm{II}} = 1$ here. Equation (4.19) is regarded as a quadratic equation for S_i, the other S_j for $j \neq i$ being assumed known. The station i is then swept repeatedly through the interval $2 \leqslant i \leqslant K-1$. At the end of each sweep the unknown vorticity $\bar{\Omega}$ is updated as in step (E) above (with, again, $R_n \equiv 0$), to ensure the conditions (3.6b); also, for symmetric solutions we impose $S(X) = S(-X)$ then, for $0 \leqslant X \leqslant 1$; this is bypassed in the possible nonsymmetric cases, of course. The alternative scheme proved faster than the original one, but attempts to extend the alternative scheme to the full massive-eddy problem have proved only partly successful so far, producing converged results only for $C_{\mathrm{II}} \leqslant 0.3$. Moreover, the massive- and thin-eddy results from both schemes agreed with each other to high accuracy, anyway, for the symmetric solutions up to $C_{\mathrm{II}} = 0.3$; not surprisingly, the sets of possible nonsymmetric solutions generated by the two schemes, in the thin-eddy case, appeared to be different from each other.

The *symmetric* solutions from scheme (A)–(F) for the massive-eddy problem are presented in Figure 2. Nearly converged *nonsymmetric* solutions *, obtained for the thin-eddy problem either from (A)–(F) or from the alternative scheme just mentioned, and obtained for the massive-eddy problem from scheme (A)–(F) alone, are shown in Figure 3. A further check on accuracy in the calculations is given in Figure 4, for the symmetric thin-eddy case. In that case the coefficient s_0 in the local behaviour $S \sim s_0(1 \pm X)^{3/2}$ of $S(X)$ as $|X| \to 1-$ can be expressed in the convergent integral from

$$s_0 = \frac{-2^{3/2}}{3\pi}\left[\int_{-1}^{1}\left\{\frac{p(\xi)}{(1-\xi)^{\frac{1}{2}}} - \frac{1}{2^{\frac{1}{2}}}\right\}\frac{\mathrm{d}\xi}{(1+\xi)^{3/2}} - 1\right], \tag{4.20}$$

from (3.6) or its inverse as in this section. The behaviour implied by (4.20), which is dependent on the global solution, is compared locally in Figure 4 with the direct

* More recent computations, however, performed for more (up to 10000) sweeps of the scheme (A)–(F), and for a range of values of C_{II}, show the solutions with nonsymmetric starting forms tending very closely indeed to the symmetric results eventually, near convergence; the nonsymmetric and the symmetric forms in fact are indistinguishable then to about four significant figures. This adds weight to the view, expressed earlier in this section, that there may well be only symmetric solutions, at least for most values of C_{II}.

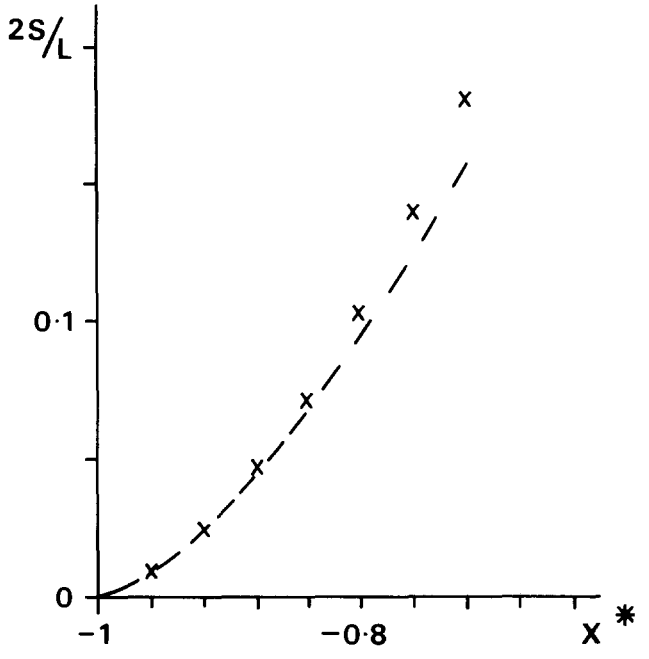

Figure 4. Comparison between the local numerical solution (×) and the analytical form $s_0(1+X^*)^{3/2}$ (— — —, with s_0 given in (4.20)), for the eddy shape near the end $X^* = -1$ in the thin-eddy symmetric case. In this calculation we took $K = 51$ and (4.20) then gave the value $s_0 = 1.0611$ from a trapezoidal integration.

numerical solution obtained previously (with $K = 51$). The agreement is found to be very close as $X \to -1$.

5. Further discussion

The following points are mainly in addition to those of the preceding sections.

(i) Another view of the physical mechanisms associated with massive-scale eddies comes from examining smaller-scale separations, and this can be more directly useful in practical terms, for many separated airfoil flows for example. Smaller-scale separations can be described completely, within an interactive framework of the triple-deck kind or similar, and so they provide a platform for moving outwards, as it were, towards the massive-scale separated cases of interest.

This means adopting an interacting boundary-layer or similar approach at finite Re or going back to triple-deck sizes of flow configurations, as the principal examples for $\mathrm{Re} \gg 1$. These latter sized flows are governed by the boundary-layer equations

$$\frac{\partial U}{\partial \bar{X}} + \frac{\partial V}{\partial \bar{Y}} = 0, \quad U\frac{\partial U}{\partial \bar{X}} + V\frac{\partial U}{\partial \bar{Y}} = -\frac{\mathrm{d}P}{\mathrm{d}\bar{X}} + \frac{\partial^2 U}{\partial \bar{Y}^2} \tag{5.1}$$

in the lower deck closest to the surface, subject to the boundary conditions

$$U = V = 0 \quad \text{at } \bar{Y} = 0 \quad \text{(or other surface conditions)} \tag{5.2}$$

$$U \sim \bar{Y} + A(\bar{X}) + f(\bar{X}) \quad \text{as } \bar{Y} \to \infty \tag{5.3}$$

and to the pressure-displacement interaction law, for subsonic motion,

$$P(\bar{X}) = \frac{1}{\pi} \int_{-\infty}^{\infty} \frac{\mathrm{d}A}{\mathrm{d}\xi} \frac{\mathrm{d}\xi}{(\bar{X}-\xi)}. \tag{5.4}$$

In (5.3) $f(\bar{X})$ denotes the scaled surface shape, be it a hump, a step, a corner or the trailing-edge shape.

Nonlinear solutions (see references in Messiter [5], Smith [9]) for separating flows can be derived numerically for increasing disturbance size, α say. Here $\alpha = 0(|f|)$ is the typical height of the hump or step, or the angle of incidence in trailing-edge flow, or the ramp angle in the central example of supersonic ramp flow, for instance. In supersonic flow (5.4) is replaced by Ackeret's law,

$$P(\bar{X}) = -\frac{\mathrm{d}A}{\mathrm{d}\bar{X}}. \tag{5.5}$$

The numerical solutions are useful for finite values of α anyway, for example in investigating trailing-edge stall, and as α increases they should move towards the massive separation cases, creating much larger scale eddies. The calculations become more difficult and prone to divergence as α increases, however, and windward differencing and multisweeping, in the forward and possibly the reversed sense also, seem essential in finite-difference methods. Much further investigation is required numerically into these increased-scale separating motions.

Some reasonable theoretical conjectures may be made about the large-α behaviour of the separating motions. Once such is the extended Kirchhoff form (see the reviews above) but that appears to hit an inconsistency at eddy closure much like the one described in Section 2. The other main contender is a massive-eddy account, like that in Section 3. This is especially encouraging since the system of triple-deck equations (5.1)–(5.4) admits the Benjamin-Ono equation (3.6a) again, for the eddy shape S in *subsonic* flow, under the assumption of a predominately inviscid eddy or eddies much greater than the typical obstacle size α. So the previous inviscid, thin-eddy, solutions of Sections 3 and 4 and Figure 2 can apply. They can also be extended to incorporate the surface-shape effect $f(\bar{X})$ if the eddy size is reduced to $O(\alpha)$, in which case we have a more Prandtl-Batchelor type of flow. The viscous parts of the large-α solution still need to be investigated carefully, to pin the solution down, and the join to the massive-separation cases studied previously still has to be followed through, but overall the large-α structure seems to be not inconsistent at this stage.

By contrast, the *supersonic* or *hypersonic-limit* regimes do not work in the same way, even at the inviscid level (Smith [9]). For, in supersonic flow for instance, with (5.5) holding, we obtain for the massive-eddy balance the steady Burgers equation

$$\tfrac{1}{8}\bar{\Omega}^2 S^2(\bar{X}) - C_{\mathrm{II}} = \frac{\mathrm{d}S}{\mathrm{d}\bar{X}} \tag{5.6}$$

in place of (3.6a). The equation (5.6) admits no closed-eddy solutions and neither does its hypersonic-limit counterpart where $\mathrm{d}S/\mathrm{d}\bar{X}$ is replaced by $S(X)$. On the other hand, analysis by Burggraf and Smith [2] shows that if the effect of the surface shape is included then the inviscid eddy can be closed. So the implication is that for these regimes the eddy

size is probably much less than in the subsonic regime. Moreover, the structure takes on the Prandtl-Batchelor form in essence. There is a difficulty, even so, because the start of the eddy ahead of a supersonic ramp requires a large pressure rise, on inviscid reasoning, and this contradicts the O(1) pressure rise ($P \approx 1.8$) known to occur in the viscous free-interaction separation upstream. Therefore, in this flow, either the proposed inviscid structure should be modified (it clearly needs to incorporate the secondary separations which can be expected in any case), or the free-interaction separation is nonunique and can lead (e.g.) to an arbitrarily large pressure rise. The latter prospect is an intriguing one and has still to be addressed. Again, the alternative of large-α separating flow produced by a backward-facing step or a ramp of finite length shows more immediate hope of fitting together with the above account, since a very large pressure variation can be built up, before the start of the step or ramp, by means of the alternative attaching-flow free-interaction.

(ii) Despite the comments in Sections 2 and 3 free-streamline theory of the extended Kirchhoff kind still "works" in the numerical and practical sense (see Messiter [5], Smith [9]) at the medium Reynolds numbers where external flow remains laminar; moreover it appears to be self-consistent in internal motions through pipes and channels and in cascade flows.

(iii) With regard to the main inviscid massive-eddy problem, the present study addresses (Sections 3 and 4) the possibility that, in addition to the symmetric solutions throughout, nonsymmetric solutions may exist which are skewed in the $\pm x$ direction, thus introducing an extra degree or degrees of freedom; see also an earlier footnote. The computations in nonsymmetric cases were only very slowly convergent, however, and so a firm statement on their existence or not is difficult to support (as yet). Note also that although the linear integral equation obtained by linearization about the symmetric solutions of (3.6a, b) (e.g.) is of a kind considered briefly in Mushkilishvili's book the coefficients involved tend to limit the amount of analytical progress. One might also conjecture that further nonsymmetry is possible with respect to the lateral direction y, expect for (say) eddies adjoining solid surfaces as in the thin-eddy triple-deck cases in (i) above. To some extent the conjectured nonsymmetry may be a side issue but the implications of this possible extra freedom existing at the inviscid level are currently being considered especially for their impact on the important viscous-periodicity condition and on the body-scale flow (the second and third tasks mentioned in Section 3).

(iv) For axisymmetric separating flow past a blunt axisymmetric body the analogue of Sections 2–4 can also be constructed. This is being considered by Mr. R. Avis in Ph.D. research at University College. In particular the slender-eddy limit, analogous to the thin-eddy limit in Section 3, yields a surface pressure

$$p_{\mathrm{I}} \propto (S^2)'' \tag{5.7}$$

from axisymmetric linearized-flow properties, with unknown eddy radius $S(X)$, while the vorticity argument inside the slender eddy now gives

$$p_{\mathrm{II}} = C_{\mathrm{II}} - \bar{a}^2 S^4, \tag{5.8}$$

where $\bar{a}$ is a constant. Equating the two pressures then produces an integrable nonlinear differential equation for the area function $\propto S^2$. Solutions with closed eddies are again found to exist.

(v) The stability properties of both the small- and the large-scale separated flows are of much theoretical and practical concern. Further, there is a clear need to develop the theory to encompass nonlinear unsteady flows, and three-dimensionality, with a view to making a connection with the Karman vortex trail observed in practice at higher Re, among other things. Some aspects of this are discussed by Smith [10].

(vi) There is also much still to be done for the inclusion of turbulent-modelled boundary layers as opposed to laminar ones. This inclusion is significant because otherwise it is tempting to appeal to turbulence effects to justify the use of rather arbitrary inviscid outer solutions.

(vii) In all the flows discussed, although there is still quite a long way to go to complete the theory, it seems that viscous forces play a most important role. Inviscid solutions can be obtained fairly readily in principle, and there is often an infinity of them available; but viscous effects narrow the choice considerably. This applies throughout small- or large-scale separated flow theory, whether the flow is governed by the Navier-Stokes or the interactive boundary-layer equations. We would presume that this important role of viscosity applies also to the nonsymmetric extra inviscid solutions (see also the earlier footnote) considered in the present study, if they exist.

Acknowledgement

Thanks are due to Dr M.J. Werle (United Technologies Research Center, East Hartford, Connecticut) and to Dr R.E. Whitehead (U.S. Office of Naval Research) for their interest in this research, which I dedicate to the memory of the late Professor R.T. (Tom) Davis.

References

[1] Fornberg, B., Steady viscous flow past a circular cylinder up to Reynolds number 600, *J. Comp. Phys.* 61 (1985) 297–320.

[2] Burggraf, O.R. and Smith, F.T., 1984–86, work in progress.

[3] Davis, R.T., A procedure for solving the compressible interacting boundary-layer equations for subsonic and supersonic flows, *A.I.A.A. paper* (1984) no. 84-1614 (presented at Snowmass, Col., U.S.A., July 1984).

[4] Ingham, D.B., 1984–85, private communications.

[5] Messiter, A.F., Boundary layer interaction theory, *Trans. Am. Soc. Mech. Eng.* 50 (1983) 1104–1113.

[6] Pierrehumbert, R.T., A family of steady, translating vortex pairs with distributed vorticity, *J. Fluid Mech.* 99 (1980) 129–144.

[7] Sadovskii, V.S., Vortex regions in a potential stream with a jump of Bernoulli's constant at the boundary, *Prikl. Math. Mech.* 35 (1971) 773–779. (transl. *Appl. Math. Mech.* 35 (1971) 729).

[8] Smith, F.T., A structure for laminar flow past a bluff body at high Reynolds number, Utd. Tech. Res. Cent. Rept. (1984) UTRC 84-31.

[9] Smith, F.T., Theoretical aspects of steady and unsteady laminar separation, *A.I.A.A. paper* (1984) no. 84-1582 (presented at Snowmass, Col., U.S.A., July 1984).

[10] Smith, F.T., Nonlinear effects and non-parallel flows; the collapse of separating motion, Proc. Symp. on stability of spatially-varying and time-dependent flows, NASA Langley Res. Cent., Virginia, U.S.A., August 1985 (to be published by Springer-Verlag). Also, rept. UTRC 85-55.

[11] Smith, F.T., A structure for laminar flow past a bluff body at high Reynolds number, *J. Fluid Mech.* 155 (1985) 175–191.

[12] Veldman, A.E.P. and Dijkstra, D., A fast method to solve incompressible boundary-layer interaction problems, Proc. 7th Int. Conf. Num. Meth. Fluid Dyn. (1980), Stanford, U.S.A.